23rd ABCM International Congress of Mechanical Engineering
December 6-11, 2015, Rio de Janeiro, RJ, Brazil

THERMAL ANALYSIS OF FRESNEL CONCENTRATOR

José Lopes da Silva Junior
Federal University of Rio Grande do Norte, Mechanical Engeneering, University Campus, L. Nova 59078970, Natal, RN, Brazil.
jlopes.jr92@gmail.com
Gabriel Ivan Medina Tapia
Federal University of Rio Grande do Norte, Mechanical Engeneering, University Campus, L. Nova 59078970, Natal, RN, Brazil.
gmedinat@ct.ufrn.br
João Gutemberg Barbosa de Farias Filho
Federal University of Rio Grande do Norte, Mechanical Engeneering, University Campus, L. Nova 59078970, Natal, RN, Brazil.
joao.gutemberg.farias@gmail.com

Abstract. *The Linear Fresnel Reflector (LFR) system is a promising technology that concentrates solar energy that is characterized by potentially be more economical as well as using smaller areas of occupied land. In LFR system a set of mirrors reflects sunlight focusing it into a stationary absorber that consists in a set of parallel tubes inside a trapezoidal cavity, that receives the flow of solar energy from the mirrors below it increasing the temperature of the fluid that passes through the tubes. The focus of this paper is to perform a Steady State thermal analysis of Fresnel concentrator. The developed model allows to simulate the variation of the fluid temperature and other parameters for different conditions of solar radiation. An attentive analysis will find great working points that can be used to develop a better LFR system.*

Keywords: *LFR, solar energy, heat transfer.*

1. INTRODUCTION

The Linear Fresnel Reflector (LFR) system is a Concentration Solar Power (CSP) technology that converts solar power in electricity through an indirect process. The LFR technology has several advantages over other CSP systems, like Parabolic Trough Solar Collector system, such as lower cost of assembly and maintenance, low structural support and reflector costs, using smaller areas of occupied land (Cau and Cocco, 2014), among other advantages.

The LFR system consists of a set of flat mirrors that reflect the incoming solar radiation focusing it into a fixed absorber that consists in a set of parallel tubes inside a trapezoidal cavity. A model of the absorber with his mechanisms of heat loss is shown in Fig.1. Inside the trapezoidal cavity, external to the tubes, contains air which is not in contact to the ambient due the glass cover below the receiver. The working fluid flows through the tubes inside the cavity absorbs heat from the reflected solar rays from the LFR field. The fluid increases its temperature due to the heat absorbed and then passing to the thermodynamic power generation cycle, usually Rankine or Organic Rankine Cycle.

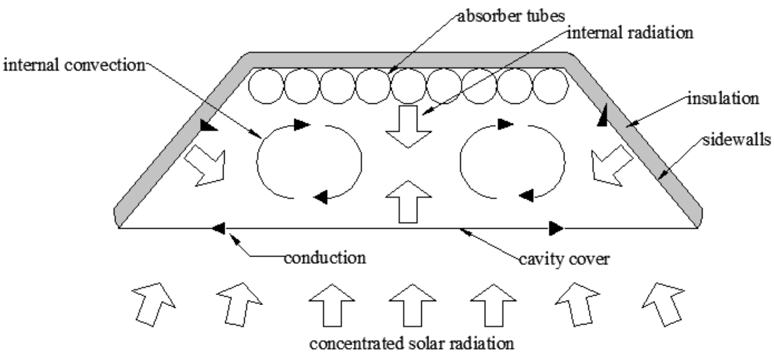

Figure 1. Model of the absorber with his mechanisms of heat loss (Zhul *et al*., 2013).

In the system, each mirror has a tilt and each one of them has a tracking system in relation to the sun aligned along the North-South direction which allows following the sun's path from East to West and reflecting the solar radiation at the same focal point, the absorber.

For power generation, where high temperatures are required, this system has a lower cost compared to other solar concentration systems, and has better reliability. Another characteristic of this system is that the reception of energy for power generation is the biggest per unit of occupied area, which is very important in countries where there is lower availability of land.

Nomenclature

U	Overall heat loss coefficient, W/m² K	T_i	Inlet fluid temperature, K
U_{L1}	Convection and radiation heat loss coefficients, W/m² k	T_o	Outlet fluid temperature, K
		T_a	Ambient temperature, K
U_{L2}	Conduction heat loss coefficient, W/m² K	T_h	Temperature of the hot pipe/plate, K
A_p	Surface area of the absorber pipe/plate facing cavity, m²	T_c	Temperature of the cold plate/glass cover, K
		T_f	Temperature of the working fluid, K
A_{cg}	Surface area of the glass cover, m²	T_R	Temperature ratio.
A_r	Reflector area, m²	T_p	Average absorber pipe/plate temperature, K
A_i	Inner surface area of the tube, m²	i	Enthalpy, J/kg
A	Inner cross section area of the tube, m²	g	Acceleration due to gravity, m²/s
x	Steam quality	k	Thermal conductivity, W/m K
$\dot{m}$	Mass flux, kg/s	DNI	Direct Normal Irradiation, W/m²
c	Specific heat, J/kgK	q''_{in}	Input heat flux, W/m²
h_l	Internal convective heat transfer coefficient of the fluid, W/m² K	q''_{loss}	Heat loss flux, W/m²
		v	Velocity, m/s
h_{cp}	Convection heat transfer coefficient from absorber pipe/plate, W/m² K	n_t	Number of tubes
		f	Frictional factor
h_{co}	Convection heat transfer coefficient from outer glass cover to air, W/m² K	*Greek symbols*	
		σ	Stefan-Boltzman constant, 5.667x10^{-8} W/m² K^4
h_{rp}	Radiation heat transfer coefficient from absorber pipe/plate to outer cover, W/m² K	ρ_{glass}	Reflectivity of the mirrors
		γ	Solidity factor
h_{ro}	Radiation heat transfer coefficient from outer glass cover to air, W/m² K	$\tau\alpha$	Transmissivity and abosorptivity coefficient
		θ_n	Angle made by mirrors with horizontal axis
Nu_c	Nusselt number for convection heat transfer.	∂z	Cell length, m.
Nu_R	Nusselt number for radiation heat transfer.	ϕ^2_{fr}	Two phase multiplayer
N_{Rc}	Radiation conduction interaction parameter.	τ_w	Shear stress, Pa
Gr	Grashof number.	ε_d	surface roughness
Re	Reynolds number.	ε_h	Emissivity of the hot plate surface of the cavity
Pr	Prandtl number.	ε_c	Emissivity of the cold plate surface of the cavity
P	Perimeter of the tube, m	ε_b	Emissivity of wall surface at the right side of the cavity.
l	Thickness of wall, m		
L	Length of the absorber (tubes), m	ε_t	Emissivity of wall surface at the left side of the cavity.
D	Depth of the cavity, m		
L_{co}	Characteristic length of outer glass cover, m	β	Thermal expansion coefficient
L_c	Characteristic length of the absorber cavity (depth), m	ρ	Density of the fluid, kg/m³
d_i	Inner diameter of the tube, m	μ	Viscosity of the fluid, N s/m²
d_o	Outer diameter of the tube, m		

In the present work, a thermal analysis is performed in the LFR absorber tubes to simulate the variation of the fluid temperature for different conditions of solar radiation. A one dimensional, steady state convective flow boiling in long, uninterrupted straight tubes which are used in LFR solar system is discussed. To simulate the variation of the working fluid temperature for different conditions of solar radiation, the developed model takes into account the variable net heat flux along the length of the tube.

2. SETUP DESCRIPTION

The LFR system taken into consideration in this paper consists of a trapezoidal cavity receiver filled with air as shown in Fig. 1, the bottom cover of the cavity is made in glass to minimize the convective heat loss and has 500 mm in width, and the depth of the cavity has 100 mm. The other three sides of the cavity are insulated with glass wool to reduce the heat loss, the thickness of the top and side walls is 25 mm, and the top wall has 300 mm in width. Inside the cavity there eight parallel receivers tubes, made in stainless steel (SS304), the outer diameter of the tube is 33,4 mm and the inner diameter is 26,7 mm. The reflectors consists in flat mirrors arranged in 6 rows parallel to the absorber, each one has 1,8 m width along the entire length of the absorber, that is 385 m. The reflectors are positioned 1 m from the ground and the absorber is positioned 13 m from the ground. The reflector arrangement is shown in Fig. 2.

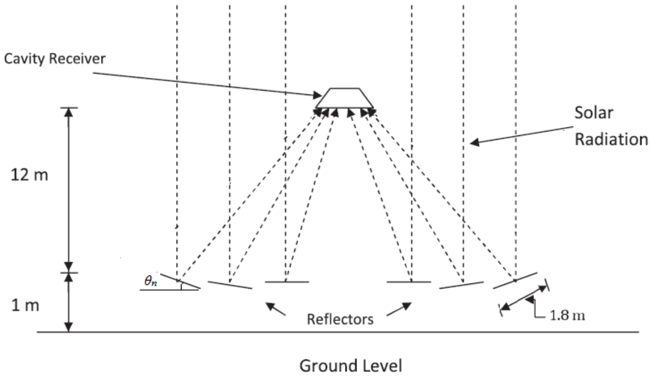

Figure 2. LFR system setup.

The mirrors reflect the solar radiation to the receiver, the reflected rays pass through the glass cover and are incident on the absorber tubes. Water gets heated while flowing through the tubes by the heat flux from the mirrors placed next the ground, and then passing to the thermodynamic power generation cycle. A resume of the proposed specifications of the LFR system is shown in Tab. 1, the values are based on the work of Sahoo *et al*., 2012.

Table 1. Proposed specifications of the LFR system.

Specifications of the LFR system.

Items	Dimensions
Bottom width of the cavity	500 mm
Top width of the cavity	300 mm
Side length of the cavity	141 mm
Depth of the cavity	100 mm
No of tubes in the cavity	8
Inner diameter of the tubes	26,7 mm
Outer diameter of the tubes	33,4 mm
Absorber length	385 m
No of reflector mirrors	6
Reflector width	1,8 m
Positions of reflectors from the ground	1 m
Positions of cavity from the ground	13 m

3. MATHEMATICAL MODELING

3.1 Cavity heat loss analysis

The mirrors in the LFR system under consideration are arranged such a way that flux falling on the tubes is almost uniform. At a particular cross section, the same temperature for all tubes can be considered. With this assumption, the heat loss analysis in the cavity is carried.

The heat transfer in the trapezoidal cavity absorber involves all three modes of heat transfer, but is mainly through convection and radiation. In the cavity, natural convection occurs. However, at outside of the cavity, if air flow prevails over the glass surface, heat transfer/loss through forced convection would takes place, although in this analysis the heat loss for conduction by insulated sides is taken in consideration. The radiant exchange between the hot absorber plate and the glass cover plate of the cavity absorber may be taken as the case of heat transfer between two infinite parallel surface with different temperature.

Estimation of the overall heat loss coefficient of the cavity absorber was done by considering convection and radiation losses form the absorber plate through glass cover at bottom portion, U_{L1}, and conduction loss coefficients from insulated sides, U_{L2}.

The heat loss coefficient of absorber from bottom through convection and radiation can be given as:

$$\frac{1}{U_{L1}} = \frac{1}{h_{cp} + h_{rp}} + \frac{A_p}{A_{cg}}\left(\frac{1}{h_{co} + h_{ro}}\right) \tag{1}$$

And the heat loss coefficient by conduction from upper insulated is shown in Eq. (2).

$$\frac{1}{U_{L2}} = \frac{l}{k_{gw}} \tag{2}$$

k_{gw} is the glass wool (insulate) thermal conductivity, W/m.K.

The overall heat loss coefficient is shown in Eq. (3) and can be estimated by the estimation by cavity correlation method (Singh *et al*., 2010).

$$U = U_{L1} + U_{L2} \tag{3}$$

The correlations suggest by Balagi and Venkatesan (1994) for estimation for convection and radiation Nusselt numbers were estimated based on the Grashof number, radiation conduction interaction parameter and the emissivities of the plates as given below.

$$Gr = \frac{\beta \cdot g \cdot L_c^{\ 3} \cdot \rho \cdot (T_h - T_c)}{\mu^2} \tag{4}$$

N_{Rc} is the radiation conduction interaction parameter used to take the conduction in care to this analysis, and is given by Eq. (5).

$$N_{Rc} = \frac{\sigma \cdot T_h^{\ 4} \cdot d}{k(T_h - T_c)} \tag{5}$$

T_R is the temperature ratio, given by Eq. (6).

$$T_R = \frac{T_c}{T_h} \tag{6}$$

$$Nu_c = 0.149 Gr^{0.294} \cdot (1+\varepsilon_h)^{-0.279} \cdot (1+\varepsilon_c)^{0.182} \cdot (1+\varepsilon_b)^{-0.135} \cdot (1+\varepsilon_t)^{0.115} \cdot \left(\frac{N_{Rc}}{N_{Rc}+1} \right)^{0.272} \tag{7}$$

$$Nu_R = 0.657 Gr^{-0.0093} \cdot \varepsilon_h^{\ 0.808} \cdot \varepsilon_c^{\ 0.342} \cdot \leq (1+\varepsilon_b)^{0.199} \cdot (1+\varepsilon_t)^{-0.039} \cdot (1+T_R^{\ 4})^{1.149} \cdot N_{Rc}^{\ \ 1.051} \tag{8}$$

The convection and radiation Nusselt number obtained from above correlations were used to calculate convection heat transfer coefficient between absorber plate and inner glass cover surface, h_{cp}, and radiation heat loss between absorber plate and glass cover, h_{rp}, as shown respectively in Eq. (9) and Eq. (10). The estimation of the convection and radiation heat loss coefficients from outer glass cover surface of the cavity, h_{co} and h_{ro}, are shown in Eq. (11) and Eq. (12), respectively. With all these coefficients is possible calculate the overall heat loss coefficient, *U*.

$$h_{cp} = \frac{Nu_c \cdot k_a}{L_c} \tag{9}$$

k_a is the thermal conductivity ok the air, W/m.K.

$$h_{rp} = \frac{\sigma (T_p^{\ 2} + T_c^{\ 2}) \cdot (T_p + T_c)}{\frac{1}{\varepsilon_c} + \frac{1}{\varepsilon_p} - 1} \tag{10}$$

T_p is the absorber temperature that was obtained by taking average of inlet and outlet fluid temperature

$$h_{co} = \frac{Nu_c \cdot k_a}{L_{co}} \tag{11}$$

$$h_{ro} = \sigma \cdot \varepsilon_c \cdot (T_c^{\ 2} + T_a^{\ 2}) \cdot (T_c + T_a) \tag{12}$$

The ambient Temperature, T_a, was over the city of Natal, Rio Grande do Norte – Brazil, obtained in the National Institute of Spatial Researches (INPE).

3.2 Convective flow analysis in the absorber tubes

As described earlier, LFR absorber tube consists in a set of horizontal tubes (eight in this work), through which water enters at sub cooled temperature and gets heated and as wet steam. The region from the inlet to the point where the working fluid temperature reaches saturation is called single phase region and the rest of the tube from that point is the two phase region. The model developed in this work is based in the following assumptions.

- The gap between the tubes is neglected. Also, it is considered that the absorber tube is a long interrupted straight tube.
- The LFR system is designed so that the heat flux is almost the same in all the tubes. Then, the heat flux received by each tube is calculated by dividing the total reflective flux from the mirrors by the number of tubes.
- One dimensional heat transfer analysis.
- The analysis is being carried out along a long, straight tube, and focus of the study is on outlet working fluid temperature, detailed analysis of subcooled and partial boiling is not considered in the present study.
- The exit condition of the steam is wet or dry. Superheating and instability issues are not considered in this study.

A steady subcooled fluid-flow enters the absorber tube with known thermodynamic state and a mass flux such as to cause a turbulent flow. A pump insures that the fluid-flow into the tubes is turbulent and developed. The tube is subject to uniform heat in flux on its outer surface and varying heat loss along the length of the tube in the single phase region. In the two phases region, as boiling occurs, the net heat flux is almost constant.

The input heat flux is shown in Eq. (13) and it takes into account the direct normal irradiation, reflector mirrors characteristics and tubes characteristics.

$$q''_{in} = \frac{DNI \cdot \rho_{glass} \cdot (\sum A_r \cos\theta_n) \cdot \gamma \cdot (\tau\alpha)}{n_t \cdot \pi \cdot d_o \cdot L} \tag{13}$$

The values of Direct Normal Irradiation, *DNI*, used in this work were over the city of Natal, Rio Grande do Norte – Brazil, using the data obtained in the work of Porfírio and Ceballos, 2013.

The heat loss flux, shown in Eq. (14), is the product between the overall heat loss coefficient discussed in Section 3.1 and the temperature difference between the outer wall of the tube and the ambient.

$$q''_{loss} = U(T_h - T_a) \tag{14}$$

To study the behavior of the working fluid temperature and pressure drop along the length of the absorber it is necessary to know the momentum balance and the energy balance, Eq. (15) and Eq. (16) shows the momentum and energy equation, in a general form.

$$-\frac{dp}{dz} = \frac{1}{A}\frac{d(\rho_h A u_h^2)}{dz} + \tau_w \frac{P}{A} \tag{15}$$

$$\dot{m}\frac{de_h}{dz} = (q''_{in} - q''_{loss})P \tag{16}$$

The subscript *h* in these equation means homogeneous quantities, in the single phase region, where the steam quality is taken to be zero, the subscript *h* should be treated as *l* (liquid). The equations to enthalpy and density are represented in Eq. (17) and Eq. (18), respectively.

$$i_h = i_l + x(i_g - i_l) \tag{17}$$

$$\rho_h = \rho_l + x(\rho_g - \rho_l) \tag{18}$$

Where the subscripts *l* and *g* represents liquid and gas, respectively.

The shear stress, τ_w, for single phase flow is:

$$\tau_w = \frac{1}{2} f \frac{\dot{m}^2}{A^2 \rho_l} \tag{19}$$

The friction factor, *f*, to single phase region can be estimated by Swamee and Jain correlation (1976) for turbulent flow.

$$f = \frac{0.25}{\left[\log_{10}\left(\frac{\varepsilon_d}{3.7 d_i} + \frac{5.74}{\mathrm{Re}^{0.9}}\right)\right]^2} \tag{20}$$

The shear stress, τ_w, in two phase region takes in consideration the two phase multiplayer, ϕ_{fr}^2, and is given by:

$$\tau_w = \frac{1}{2} f_{lo} \frac{\dot{m}^2}{A^2 \rho_l} \phi_{fr}^2 \tag{21}$$

Where

$$f_{lo} = \frac{0.079}{\mathrm{Re}^{0.25}} \tag{22}$$

The two phase multiplayer, ϕ_{fr}^2, is given by Friedel correlation, because, based on Pye (2008), this correlation gives better prediction than others correlations .

The Eq. (23) is can be obtained by using convection and conduction resistance between outer surface of the tube wall and the fluid. This equation shows the working fluid temperature in terms of the outer wall of the tube (temperature of the hot pipe).

$$(q''_{in} - q''_{loss})P = \frac{T_h - T_f}{\frac{1}{2\pi k_s} \cdot \ln\left(\frac{d_o}{d_i}\right) + \frac{1}{h_l \pi d_i}} \tag{23}$$

k_s is the thermal conductivity of the tube material, W/m.K.

The convective heat transfer coefficient of the bulk fluid, h_l, can be found by the Dittus-Boelter correlation in the single phase region, this correlations is showed in Eq. (24). In the two phase region, the heat transfer coefficient for liquid, h_l, only can be calculated using the Dittus-Boelter correlation assuming the liquid fraction inside the tube, as showed in Eq. (25). The choice of these equations is based on Odeh *et al*., 1998, who reports that these equations gives better prediction for long, straight and horizontal tube applications, like LFR.

$$h_l = 0.023 \mathrm{Re}^{0.8} \mathrm{Pr}^{0.4} \frac{k}{d_i} \tag{24}$$

$$h_l = 0.023 \left(\frac{G(1-x)d_i}{\mu_l}\right)^{0.8} \mathrm{Pr}^{0.4} \frac{k}{d_i} \tag{25}$$

Where G is the mass flux per unit area, kg/m²s.

3.3 Solution procedure

The Eq. (15) and Eq. (16) are non-linear coupled firs order Ordinary Differential Equations. These equations discretized by implicit first order finite difference method in the single phase region, generating the equations below:

$$\frac{p_{z+1}-p_z}{\partial z}-\frac{1}{A}\frac{\left[(\rho_l A u_l^2)_{z+1}-(\rho_l A u_l^2)_z\right]}{\partial z}-\tau_w\frac{P}{A_i}=0 \tag{26}$$

$$\dot{m}\frac{\left[c(T_{z+1}-T_z)+\dfrac{u_{l,z+1}^2-u_{l,z}^2}{2}\right]}{\partial z}-\ q''_{in}-U(T_h-T_a)\ P=0 \tag{27}$$

The computational domain is divided in a number of cells of equal length, ∂z. At each cell Eq. (23), Eq. (26) and Eq. (27) are solved for T_{z+1}, T_{wo} and p_{z+1} by the Newton method. The fluid properties are calculated based on the mean temperature of the cell. The iterations are carried out until residuals of equations are below 10^{-3}.

In two phase region (from the point where the working fluid temperature becomes equal to saturation temperature until the end of the tube) the equations discretized by implicit first order finite difference method are showed in Eq. (28) and Eq. (29).

$$\frac{p_{z+1}-p_z}{\partial z}-\frac{1}{A}\frac{\left[(\rho_h A u_h^2)_{z+1}-(\rho_h A u_h^2)_z\right]}{\partial z}-\tau_w\frac{P}{A_i}=0 \tag{28}$$

$$\dot{m}\frac{\partial}{\partial z}\left[\left[[i_l+x(i_g-i_l)]_{z+1}-[i_l+x(i_g-i_l)]_z\right]+\frac{u_{h,z+1}^2-u_{h,z}^2}{2}\right] \\ -\ q''_{in}-U(T_h-T_a)\ P=0 \tag{29}$$

The method to solve these equations in two phase region is similar to the described early to single phase region. At each cell Eq. (23), Eq. (28) and Eq. (29) are solved for x, T_{wo}. The cell length, ∂z, was considered 1 m, this value was taken because it showed the best balance for time of computation and accuracy.

The EES (Engineering Equation Solver) software version 9.699 is used to calculate the thermodynamics and transport properties of the working fluid and the air.

4. RESULTS AND DISCUSSIONS

The overall heat loss coefficient varied with the outer wall temperature of the absorber tube is shown in Fig. 3. The results obtained are in accordance with the work of Singh *et al.*,2010 showing the increased of the overall heat loss coefficient by increasing the outer wall temperature of the absorber tube.

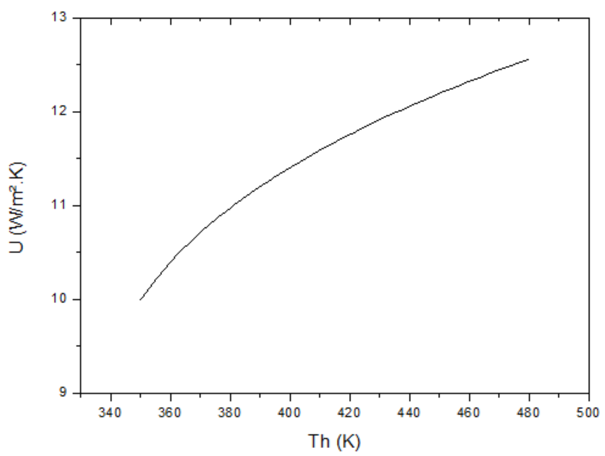

Figure 3. Overall heat loss coefficient vs. Temperature of the tube outer wall.

Figure 4 show the results of the work of Singh *et al.*, 2010. Where was plotted the overall heat loss coefficient obtained by experimental model, parallel plate correlation and cavity correlation. The differences between the values obtained in this paper and those found by Singh *et al.*, 2010 were due the differences in materials used in the cavity and some parameters considered for the specific case of Natal-RN meteorological condition in this paper.

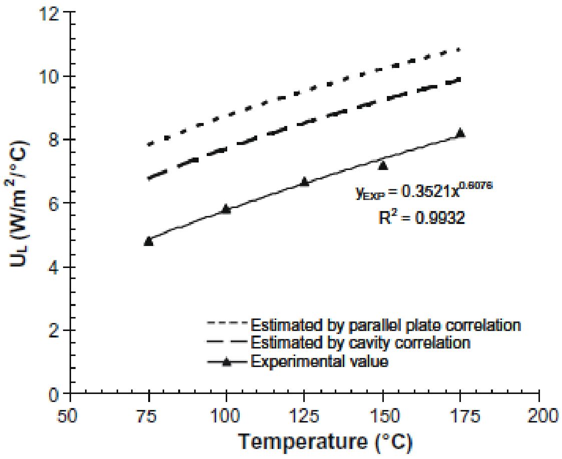

Figure 4. Overall heat loss coefficient vs. Temperature of the tube outer wall (Singh *et al.*, 2010)

The Fig. 5 shows the behavior of the bulk fluid temperature for three different values of *DNI*, namely three different conditions of solar radiation along the absorber tube length. The values of *DNI* choice in this simulation are according to the solar radiation condition in Natal – RN during the year.

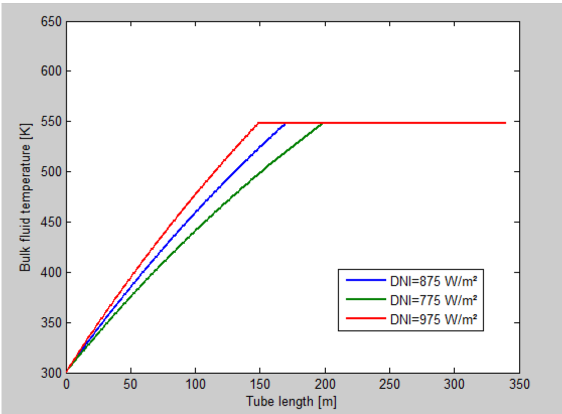

Figure 5. Bulk fluid temperature vs. Absorber tube length.

The Fig. 6 shows the steam quality along the absorber tube length for the same three solar radiation conditions showed in Fig 5.

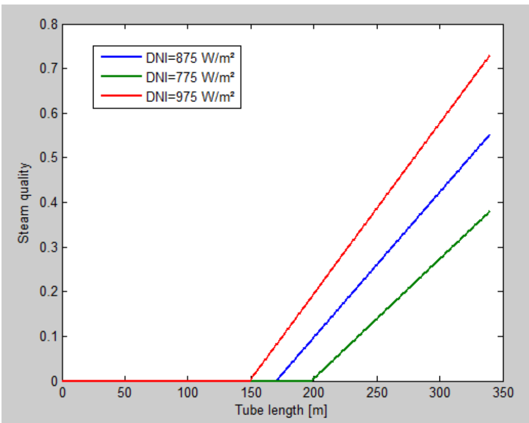

Figure 6. Steam quality vs. Absorber tube length.

In the carried out simulation was possible to note that the increasing of the direct normal irradiation, *DNI*, incident in the LFR system increases the rate of increase of the bulk fluid temperature, as possible to note in Fig. 5. Due to this, the working fluid reaches the saturation temperature in a smaller length of the tube and, consequently, a smaller single phase region. Therefore, for the same absorber length, the larger incident *DNI* implies in a driest steam delivered to the power generation cycle, due the increase of the two phase region. This behavior can be seen in Fig. 6 where the largest incident *DNI* implied in the better steam quality.

Figure 7 (a) shows the steam quality along the absorber tube length, for a tube length of 340 m and Fig. 7 (b) shows the steam quality along the absorber tube length, for a tube length of 420 m. Both figures using the same solar radiation condition, the average *DNI* value for the city of Natal – RN.

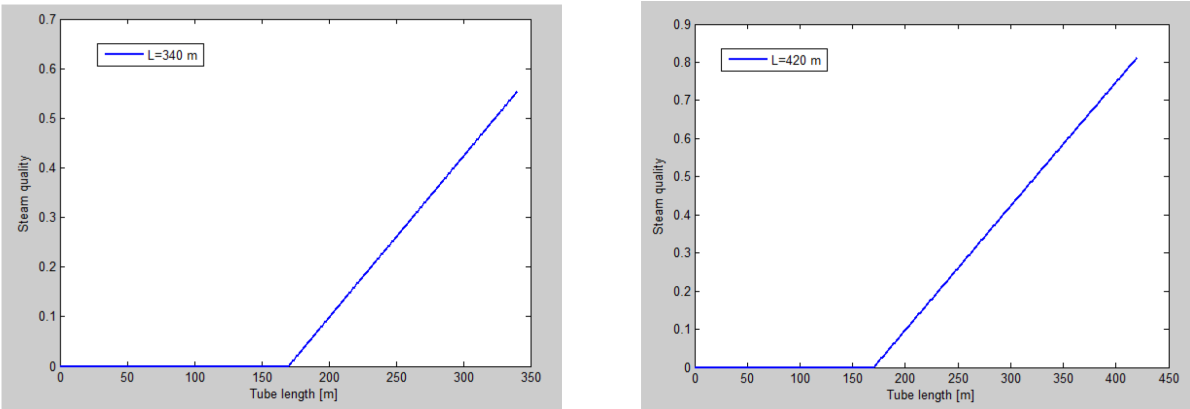

Figure 7 (a). Steam quality vs. Absorber tube length, L=340. (b). Steam quality vs. Absorber tube length, L=420 m.

Analyzing Fig 7 is possible conclude that for the same solar radiation condition, a bigger absorber tube length implies in a better steam quality. It happens because the increase of the two phase region due the increased tube length. Therefore the steam delivered to the power generation cycle will be of better quality for a bigger absorber tube length.

Figure 8 shows the pressure drop along the direction of the flow for three different conditions of solar radiation. In this simulation is possible to note that a bigger *DNI* value implies in a bigger pressure drop. It happens due the pressure drop is more severe in two phase region, and two phase region length increases with rising *DNI* value.

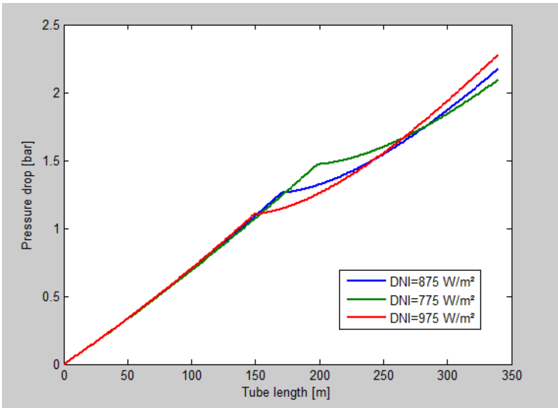

Figure 8. Pressure drop vs. Absorber tube length.

Figure 9 shows the heat loss flux along the absorber tube length. As expected the heat loss flux is lower for a smaller incident *DNI*, but this lower heat loss becomes with more time to the bulk fluid reaches the saturation temperature, that implies in a smaller two phase region and consequently more humid steam delivered to the power generation cycle.

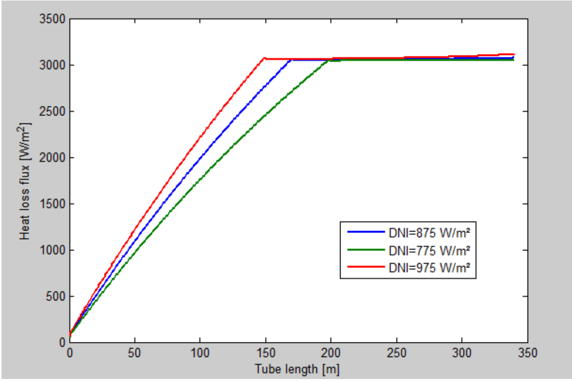

Figure 9. Heat loss flux vs. Absorber tube length.

It is also possible to conclude that the higher the *DNI*, bigger tube length and lower heat losses (provided for cavity design) will be greater LFR system efficiency, delivering high steam quality to the power generation cycle, which will also improve its performance.

5. ACKNOWLEDGEMENTS

This work was developed with the support of PRH-14 program of ANP (National Petroleum Agency) and Petrobras.

6. REFERENCES

Balaji C, Venkatesan S., 1994. *Correlations for free convection and surface radiation in square cavity*.

Cau, G. and Cocco, D., 2014. "Comparision of medium-size concentrating solar power plants based on parabolic throgh and linear Fresnel collectors". In *Proceedings of the 68th Conference of the Italian Thermal Machines Engeneering Association, ATI 2013.*

Odeh, S.D., Morrison, G.L., Behnia, M., 1998. "Modelling of parabolic trough direct steam generation solar collectors". *Solar Energy* 62, 395–406.

Porfidio, A. C. S. and Ceballos, J. C., 2013. "A method of estimating the normal direct solar radiation by geostationary satellite images: Preliminary results". In *Proceedings of Brazillian Symposium of Remote Sensing – SBSR 2013*. Foz do Iguaçu, Brazil.

Pye, J.D., 2008. "System modeling of compact linear Fresnel reflector". Ph.D. Thesis. University of New South Wales, Australia.

Sahoo, S.S., Singh, S. and Banerjee, R. 2012. *Steady state hydrothermal analysis of the absorber tubes used in Linear Fresnel Reflector solar thermal system.*

Singh, P.L., Sarviya, R.M. and Bhagoria, J.L. 2010. *Heat loss study of trapezoidal cavity absorbers for linear solar concentrating collector.*

Swamee, P.K., Jain, A.K., 1976. "Explicit equations for pipe-flow problems". *Journal the Hydraulics Division (ASCE)* 102, 657–664.

Zhul, G., Wendelin, T., Wagner, M.J. and Kustler, C. 2013. *History, current state, and future of linear Fresnel concentrating solar collectors.*

7. RESPONSIBILITY NOTICE

The authors are the only responsible for the printed material included in this paper.